LETTERS
PUBLISHED ONLINE: 8 DECEMBER 2013 | DOI: 10.1038/NGEO2020
nature geoscience

Common 0.1 bar tropopause in thick atmospheres set by pressure-dependent infrared transparency

T. D. Robinson[1,2]* and D. C. Catling[2,3,4]

A minimum atmospheric temperature, or tropopause, occurs at a pressure of around 0.1 bar in the atmospheres of Earth[1], Titan[2], Jupiter[3], Saturn[4], Uranus and Neptune[4], despite great differences in atmospheric composition, gravity, internal heat and sunlight. In all of these bodies, the tropopause separates a stratosphere with a temperature profile that is controlled by the absorption of short-wave solar radiation, from a region below characterized by convection, weather and clouds[5,6]. However, it is not obvious why the tropopause occurs at the specific pressure near 0.1 bar. Here we use a simple, physically based model[7] to demonstrate that, at atmospheric pressures lower than 0.1 bar, transparency to thermal radiation allows short-wave heating to dominate, creating a stratosphere. At higher pressures, atmospheres become opaque to thermal radiation, causing temperatures to increase with depth and convection to ensue. A common dependence of infrared opacity on pressure, arising from the shared physics of molecular absorption, sets the 0.1 bar tropopause. We reason that a tropopause at a pressure of approximately 0.1 bar is characteristic of many thick atmospheres, including exoplanets and exomoons in our galaxy and beyond. Judicious use of this rule could help constrain the atmospheric structure, and thus the surface environments and habitability, of exoplanets.

'Atmospheric structure' is usually taken to mean an average vertical temperature profile, which provides fundamental information about how physical and chemical processes change with altitude. In discussing atmospheric structure, the terms tropopause and radiative–convective boundary are sometimes used interchangeably. Here, we keep these terms separate because they are located at different levels in the real atmospheres that we consider, with Titan being the most extreme case. Specifically, we use 'tropopause' to mean the temperature minimum. Remote sensing and *in situ* measurements have shown that tropopauses all occur around ~0.1 bar on planets in the Solar System with thick atmospheres and stratospheric inversions (Fig. 1). No explanation exists for this common tropopause level, so we investigated its physics with an analytic one-dimensional model of atmospheric structure described in ref. 7. Dynamics can modulate the tropopause pressure with latitude[8,9], but radiative–convective equilibrium exerts first-order control of globally averaged structure.

Our model is constructed as follows. Infrared opacities are grey, that is, described by a single, broadband optical depth, $\tau_{\rm IR}$, at every pressure level. Solar radiative transfer occurs in stratospheric and tropospheric channels. Parameters $k_{\rm strato} = \tau_{\rm sws}/\tau_{\rm IR}$ and $k_{\rm tropo} = \tau_{\rm swt}/\tau_{\rm IR}$ control the attenuation of solar energy in these two channels, where $\tau_{\rm sws}$ and $\tau_{\rm swt}$ are short-wave optical depths. Tropospheric convection follows a dry adiabat adjusted by an empirical scaling factor typically around 0.6–0.9 to match an observed mean moist adiabat in each atmosphere. The ratio (γ) of specific heats at constant pressure (c_p) and volume (c_v), respectively, ($\gamma = c_p/c_v$) sets the dry adiabatic lapse rate, and is 1.4 for atmospheres dominated by diatomic gases, such as those considered here.

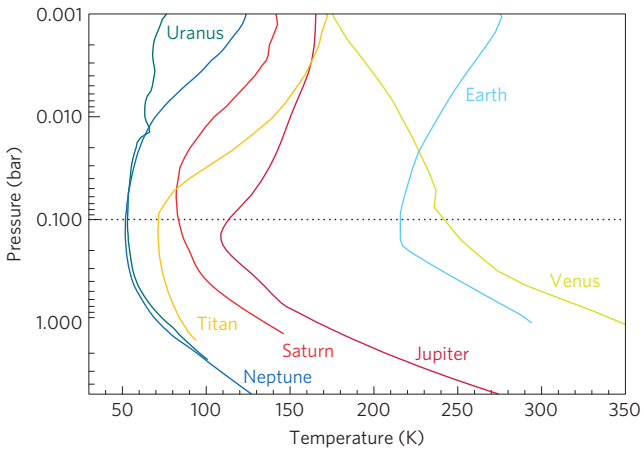

Figure 1 | Temperature–pressure profiles for worlds in the Solar System with thick atmospheres[1–4,28]. Temperature minima commonly occur around 0.1 bar. Venus has a very weak 0.1 bar tropopause in the global mean (see text). More information regarding data sources is given in the Supplementary Information.

Our model uses a known power law between pressure (p) and the grey infrared optical depth of $\tau_{\rm IR} \propto p^n$ (ref. 10). This scaling arises from combining the differential optical depth $\mathrm{d}\tau_{\rm IR} = -\kappa \rho_a \,\mathrm{d}z$ (where κ is a grey opacity, ρ_a is the absorber mass density and $\mathrm{d}z$ is the differential altitude) with hydrostatic equilibrium $\mathrm{d}p/\mathrm{d}z = -g\rho$ (where g is the gravitational acceleration and ρ is atmospheric density), so that $\mathrm{d}\tau_{\rm IR} \propto \kappa \,\mathrm{d}p$ (see Supplementary Information). Below middle stratospheres, radiative transfer is dominated by pressure-broadening and collision-induced absorption, which have $\kappa \propto p$, and, thus, $n = 2$ from integration[11]. We do not use $n = 1$, which would correspond to higher levels of the atmosphere where Doppler broadening dominates[12,13] and κ is independent of pressure (see also Supplementary Fig. 3).

Given γ, n and other inputs (Table 1), our model computes radiative–convective equilibrium by solving for infrared optical depths at the radiative–convective boundary ($\tau_{\rm rc}$) and at a reference

[1]NASA Ames Research Center, Moffett Field, California 94035, USA, [2]NASA Astrobiology Institute's Virtual Planetary Laboratory, University of Washington, Seattle, Washington 98195, USA, [3]University of Washington Astrobiology Program, University of Washington, Seattle, Washington 98195, USA, [4]Department of Earth and Space Sciences, University of Washington, Seattle, Washington 98195, USA. *e-mail: tyler.d.robinson@nasa.gov

Table 1 | Parameters and computed variables for simple models of atmospheric structure of Earth, Jupiter, Saturn, Titan, Uranus and Neptune.

World	Earth	Jupiter	Saturn	Titan	Uranus	Neptune
p_0 (bar)	1	1	1	1.5	1	1
T_0 (K)	288	166	135	94	76	72
α	0.6	0.85	0.94	0.77	0.83	0.87
$F^{\odot}_{\text{strato}}$ (W m^{-2})	7	1.3	0.41	1.49	0.24	0.09
$F^{\odot}_{\text{tropo}}$ (W m^{-2})	233	7.0	2.04	1.12	0.41	0.18
F_{i} (W m^{-2})	Minor	5.4	2.01	Minor	Minor	0.43
k_{strato}	90	90	180	120	220	580
k_{tropo}	0.16	0.06	0.03	0.20	0.08	0.20
τ_{rc}	0.15	0.34	0.44	4.4	0.62	0.41
τ_0	1.9	6.3	9.2	5.6*	8.7	3.0
τ_{tp}	0.050	0.064	0.040	0.077	0.042	0.017
p_{tp} (bar; model)	0.16	0.10	0.066	0.18	0.070	0.075
p_{tp} (bar; observed)	0.16	0.14	0.08	0.2	0.11	0.1

Parameters include a tropospheric reference pressure (p_0) and temperature (T_0), an adjustment to the dry adiabat to account for volatile condensation (α), the internal energy flux (F_{i}), the solar flux absorbed in the stratosphere ($F^{\odot}_{\text{strato}}$) and troposphere ($F^{\odot}_{\text{tropo}}$), and two parameters that control solar energy attenuation in these two channels (k_{strato} and k_{tropo}). For rocky bodies, $F^{\odot}_{\text{tropo}}$ includes surface absorption. For example, Earth has $F^{\odot}_{\text{strato}} + F^{\odot}_{\text{tropo}} = 240$ W m^{-2}, the global mean absorbed solar flux. See Supplementary Information for more information. *For Titan, $\tau_0 = 2.5$ at $p = 1$ bar.

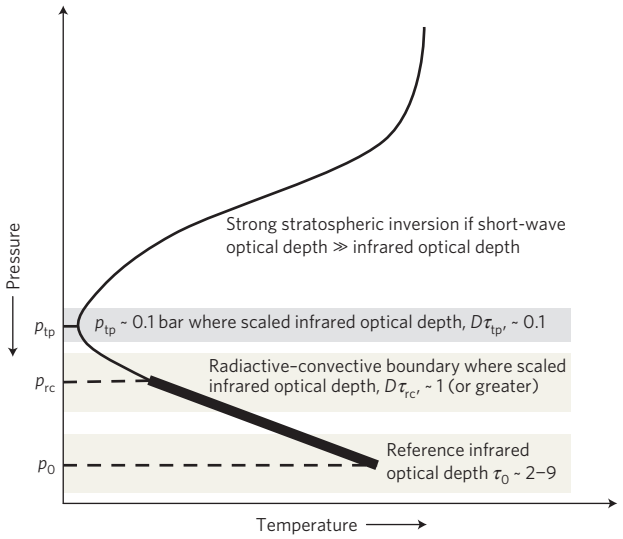

Figure 2 | Schematic diagram of thermal structure in a thick planetary atmosphere with a stratospheric inversion. A general feature is a grey infrared optical depth, τ_0, of ~2–9 at a pressure, p_0, of 1 bar. There is a radiative–convective boundary at a scaled infrared optical depth, $D\tau_{\text{rc}}$, of about unity or greater. A tropopause temperature minimum occurs at a pressure, p_{tp}, of about 0.1 bar and a scaled infrared optical depth, $D\tau_{\text{tp}}$, of about 0.1. The 'diffusivity factor' D for the optical depth is ~1.66 (see text). The thickened portion of the profile indicates the convective part of the troposphere.

pressure (τ_0, determined at either the surface or 1 bar where the atmosphere is optically thick in the infrared). The greenhouse effect necessary to maintain temperature T_0 at p_0 is related to τ_0. Consequently, the tropopause pressure, p_{tp}, weakly declines with increasing greenhouse effect according to $p_{\text{tp}} \propto \tau_0^{-1/n} \propto \tau_0^{-1/2}$, consistent with studies of Earth's contemporary warming[14].

Modelling results have common features shown schematically in Fig. 2, with precise values given in Table 1. First, tropopause pressures are all correctly computed near 0.1 bar. Second, the radiative–convective boundary is always below the tropopause. The scaled optical depth at the radiative–convective boundary is $D\tau_{\text{rc}} \approx 1$ for all worlds except Titan (the diffusivity factor, D, is ~1.66 and accounts for the integration of radiance over a hemisphere[15,16]). Titan has a very shallow convective region up to only ~1.3 bar because significant short-wave absorption in its upper hazy troposphere causes stability against convection. Third, the grey infrared optical depth at 1 bar tends to range between 2 and 10 (mean = 5.3 ± 3.2). Finally, the grey infrared optical depth of the tropopause is always about $D\tau_{\text{tp}} \approx 0.1$ (mean = 0.08 ± 0.03).

The tropopause temperature minimum occurs in the radiative regime, where an analytic expression for the temperature (Supplementary Eq. 2) allows us to assess the conditions for the minimum. Setting the derivative of the temperature profile to zero gives the infrared optical depth at the tropopause as:

$$\tau_{\text{tp}} = \frac{1}{k_{\text{strato}}} \ln\left[\frac{F^{\odot}_{\text{strato}}}{F^{\odot}_{\text{tropo}} + F_{\text{i}}}\left(\frac{k^2_{\text{strato}}}{D^2} - 1\right)\right] \quad (1)$$

Here, $F^{\odot}_{\text{strato}}$ and $F^{\odot}_{\text{tropo}}$ are the solar fluxes absorbed in the stratosphere and troposphere, respectively, and F_{i} is the internal heat flux of the planet. (For planets with surfaces, $F^{\odot}_{\text{tropo}}$ is the solar flux absorbed at the surface and in the troposphere.) Note that equation (1) does not depend on the ratio of specific heats (γ). Consequently, the inferred tropopause level is valid for thick atmospheres with tropopause minima dominated by either triatomic or diatomic gases (for example, CO_2 or H_2, respectively). The expression depends only on two parameters: the ratio $F^{\odot}_{\text{strato}}/(F^{\odot}_{\text{tropo}} + F_{\text{i}})$ and k_{strato}. The former gives the ratio of the stratospheric absorbed flux relative to that from below, which in Table 1 is highest for Titan and lowest for Earth. Essentially, k_{strato} parameterizes the effect of an arbitrary short-wave absorber through an exponential decline in heating from a stratopause.

Equation (1) yields a non-zero, physical result only when

$$k^2_{\text{strato}} > D^2\left[1 + \left(F^{\odot}_{\text{tropo}} + F_{\text{i}}\right)/F^{\odot}_{\text{strato}}\right] \quad (2)$$

which sets the threshold value of k_{strato} for the formation of a tropopause temperature minimum and stratospheric inversion. Values of k_{strato} above this threshold cause deposition of enough energy at low pressures for a stratospheric inversion. If k_{strato} is below the threshold, short-wave energy is absorbed at depths where infrared radiation primarily determines the temperature structure, thus preventing the formation of an inversion and tropopause minimum (see Supplementary Information). Typical flux ratios in this expression mean that k_{strato} must be of order ~100 for a

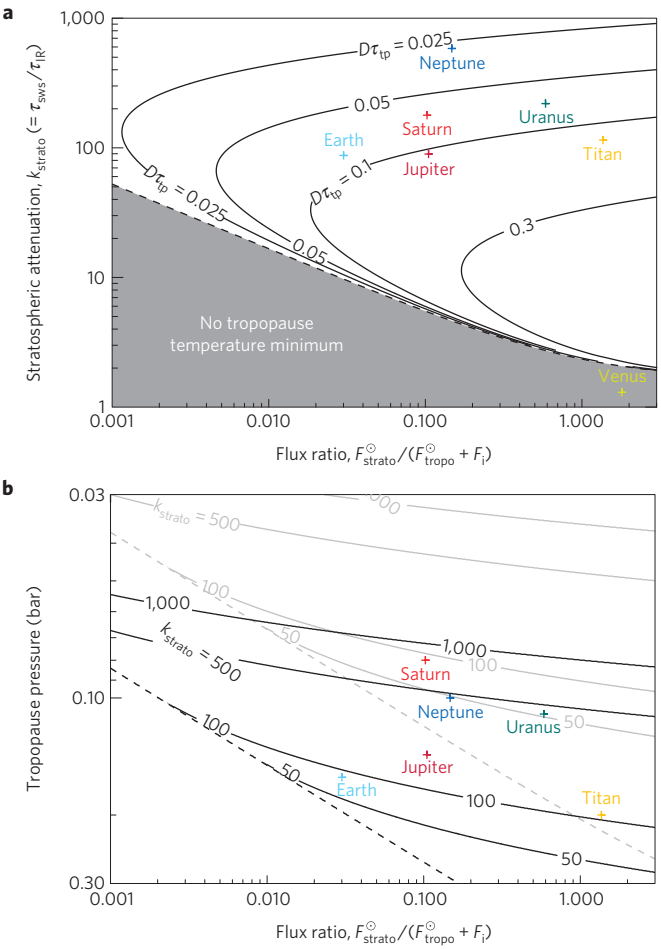

Figure 3 | Tropopause grey infrared optical depth and pressure. **a**, Contours of $D\tau_{tp}$ over a wide range of parameter space for the stratospheric attenuation strength parameter (k_{strato}) and the ratio of the stratospheric absorbed stellar flux ($F^{\odot}_{strato}$) to the sum of the tropospheric absorbed stellar flux and the internal heat flux ($F^{\odot}_{tropo} + F_i$). **b**, Tropopause pressures (from equations (1) and (3)) over a wide range of values for the ratio of $F^{\odot}_{strato}$ to ($F^{\odot}_{tropo} + F_i$). Contours are for k_{strato}, where black lines assume $\tau_0 = 2$ at 1 bar, and grey lines assume $\tau_0 = 10$ at 1 bar. Values for Solar System worlds are indicated.

well-developed minimum. In addition, the larger the internal flux, F_i, the larger k_{strato} needs to be for an inversion to exist.

Contours in a plot of stratospheric attenuation k_{strato} versus $F^{\odot}_{strato}/(F^{\odot}_{tropo} + F_i)$ show the range of $D\tau_{tp}$ for the bodies of the Solar System (Fig. 3a). The plot covers a broader range of parameter space than these bodies alone and demonstrates a general rule that worlds with relatively strong stratospheric inversions will tend to have $D\tau_{tp} \approx 0.1$ (see Supplementary Fig. 1).

Venus does not have a well-developed tropopause temperature minimum in the global average because it lacks a significant stratospheric inversion, which is consistent with our tropopause theory. However, Venus is marginal (Fig. 3a) and, in fact, possesses a distinct tropopause temperature minimum at ~0.1 bar in its mid to high latitudes[17], and so conforms to the ~0.1 bar rule when a minimum is seen (see Supplementary Information). The reason for the latitudinal variations in tropopause sharpness is unknown but may be a modulation of the radiative–convective mean state by a Hadley-like meridional circulation above the cloud tops[18]. The interpretation is complicated by the presence of unknown absorbers at 0.2–0.5 μm (ref. 19). Mars' low surface pressure of ~0.006 bar means that it does not fall within our scope of examining commonalities in thick atmospheres and so Mars is not plotted in Fig. 3a. However, the lack of a short-wave absorber (that is, $k_{strato} \ll 1$) accounts for Mars' absence of a stratospheric inversion.

Optical depths near the 1 bar pressure levels generally lie between 2 and 10 for the bodies in the Solar System; moreover line-by-line calculations justify the same range for a suite of Titan-like N_2–CH_4–H_2 atmospheres encompassing surface temperatures of 80–140 K, H_2-dominated gas giant atmospheres over a range of 1 bar reference temperatures of 75–400 K, and Earth-like N_2–H_2O – CO_2 atmospheres with surface temperatures from 250–300 K (see Supplementary Information). The Earth-like atmospheres are of particular interest for exoplanets because a 'habitable' planet is conventionally defined as one where liquid water is stable on the surface[20].

We can now see how ~0.1 bar tropopauses arise for worlds with atmospheric compositions like those of the Solar System. As pressure-broadening or collision-induced absorption applies generally to thick atmospheres, we can use the scaling between pressure and grey infrared optical depth to relate the tropopause pressure, p_{tp}, to τ_{tp} through

$$p_{tp} = p_0 \left(\tau_{tp}/\tau_0\right)^{0.5} \quad (3)$$

Using our constraint that $D\tau_{tp} \approx 0.1$ and the range of values for τ_0 at a reference pressure of 1 bar ($2 \leq \tau_0 \leq 10$), the tropopause pressure must be near 0.1 bar (for example, the average atmosphere of Table 1 has $p_{tp} \approx (0.05/5)^{0.5}$). Figure 3b uses the bounding values of τ_0 (2 and 10) at $p_0 = 1$ bar to show tropopause pressures near 0.1 bar for parameter space that encompasses and goes beyond the Solar System bodies.

As a consequence of the above calculations, we reason that a ~0.1 bar tropopause is an emergent rule that will apply to thick atmospheres on numerous exoplanets and exomoons that have compositions that are not markedly dissimilar to those in the Solar System, such as the oxidizing conditions of Earth and Venus, or the reducing conditions of Titan and the giant planets. For the latter, carbon will be in the form of CH_4, which along with photochemically generated hydrocarbons will create an inversion[21]. Amongst oxidizing stratospheres, an O_2–CO_2 atmosphere has ozone, whereas a CO_2–SO_3 Venus-like stratosphere will have elemental sulphur short-wave absorbers (ref. 21, p. 291; Supplementary Table 1).

Our hypothesis of a ~0.1 bar tropopause rule—which clearly applies only to atmospheres with stratospheric inversions—is testable. Already, observations of HD 209458b, a so-called 'Hot Jupiter' that is thought to possess a stratospheric inversion, yield rough estimates for a tropopause minimum near 0.1 bar (ref. 22). Although the rule works for Titan, which has a 16 day rotational period, it may prove inappropriate to apply globally averaged models to rotationally locked bodies, which could possess strong temperature contrasts between day and night hemispheres. Similarly, a runaway greenhouse with large infrared opacity will not satisfy equation (2) for a stratospheric inversion, so is outside the scope of our rule.

Exceptions aside, our proposed rule could help with the assessment of future telescopic spectra of exoplanet atmospheres[23,24] in many ways. For example, an algorithm for retrieving atmospheric properties has recently been applied to synthetic spectra of an Earth-like world[25]. In many cases, the retrieved tropopause pressure was near 1 bar, which was much deeper than the 0.3 bar 'target' tropopause used to generate spectra. Such algorithms could be improved by assuming a 0.1 bar tropopause as a Bayesian prior.

As a result of its applicability to Earth-like worlds, the 0.1 bar tropopause rule could help in assessing exoplanet habitability. In the future, surface pressure could be estimated from fits to exoplanet spectral features[26] whereas the surface temperature

might be obscured because of the lack of an infrared window at the wavelengths of observation. Alternatively, the surface temperature might be estimated from a spectrum whereas the surface pressure remains unknown. In either scenario, a 0.1 bar tropopause assumption in a radiative–convective model[7] would allow an estimate of surface temperature or pressure, respectively, which together are required to assess liquid water stability. The tropopause temperature would be needed. This could come from spectral features but, if not, a reasonable first-order estimate is the 'skin temperature' of $T_{\rm eff}/2^{0.25}$, where $T_{\rm eff}$ is the effective blackbody temperature of the planet (ref. 6, p. 404). For Earth, for example, $T_{\rm eff} = 255$ K and the skin temperature is 214 K, which is within a few per cent of the observed global mean tropopause at ~208 K (ref. 27).

Thus, a unity of physics not only explains ~0.1 bar tropopauses in thick Solar System atmospheres but also has the implication of potentially constraining exoplanet habitability.

Received 28 March 2013; accepted 29 October 2013; published online 8 December 2013

References

1. McClatchey, R. A., Fenn, R. W., Selby, J. E. A., Volz, F. E. & Garing, J. S. *Optical Properties of the Atmosphere* 3rd edn (Air Force Cambridge Research Labs, 1972).
2. Lindal, G. F. *et al*. The atmosphere of Titan—an analysis of the Voyager 1 radio occultation measurements. *Icarus* **53,** 348–363 (1983).
3. Moses, J. I. *et al*. Photochemistry and diffusion in Jupiter's stratosphere: Constraints from ISO observations and comparisons with other giant planets. *J. Geophys. Res.* **110,** E08001 (2005).
4. Lindal, G. F. The atmosphere of Neptune—an analysis of radio occultation data acquired with Voyager 2. *Astron. J.* **103,** 967–982 (1992).
5. Sanchez-Lavega, A. *An Introduction to Planetary Atmospheres* (CRC Press/ Taylor & Francis, 2010).
6. Goody, R. M. & Yung, Y. L. *Atmospheric Radiation: Theoretical Basis* (Oxford Univ. Press, 1989).
7. Robinson, T. D. & Catling, D. C. An analytic radiative–convective model for planetary atmospheres. *Astrophys. J.* **757,** 104 (2012).
8. Schneider, T. The tropopause and the thermal stratification in the extratropics of a dry atmosphere. *J. Atmos. Sci.* **61,** 1317–1340 (2004).
9. Haqq-Misra, J., Lee, S. & Frierson, D. M. W. Tropopause structure and the role of eddies. *J. Atmos. Sci.* **68,** 2930–2944 (2011).
10. Pollack, J. B. Temperature structure of nongray planetary atmospheres. *Icarus* **10,** 301–313 (1969).
11. McKay, C. P., Lorenz, R. D. & Lunine, J. I. Analytic solutions for the antigreenhouse effect: Titan and the early earth. *Icarus* **137,** 56–61 (1999).
12. Kondrat'ev, K. I. A. *Radiation in the Atmosphere* Vol. 12 (Academic, 1969).
13. Hanel, R. A., Conrath, B. J., Jennings, D. E. & Samuelson, R. E. *Exploration of the Solar System by Infrared Remote Sensing* (Cambridge Univ. Press, 2003).
14. Seidel, D. J. & Randel, W. J. Variability and trends in the global tropopause estimated from radiosonde data. *J. Geophys. Res.* **111,** D21101 (2006).
15. Armstrong, B. H. Theory of the diffusivity factor for atmospheric radiation. *J. Quant. Spectrosc. Rad. Transfer* **8,** 1577–1599 (1968).
16. Rodgers, C. D. & Walshaw, C. D. Polynomial approximations to radiative functions. *Q. J. R. Meteorol. Soc.* **89,** 422–423 (1963).
17. Tellmann, S., Patzold, M., Hausler, B., Bird, M. K. & Tyler, G. L. Structure of the Venus neutral atmosphere as observed by the Radio Science experiment VeRa on Venus Express. *J. Geophys. Res.* **114,** E00B36 (2009).
18. Baker, N. L. & Leovy, C. B. Zonal winds near Venus cloud top level: A model study of the interaction between the zonal mean circulation and the semidiurnal tide. *Icarus* **69,** 202–220 (1987).
19. Mills, F. P., Esposito, L. W. & Yung, Y. L. in *Exploring Venus as a Terrestrial Planet Geophysical Monograph Series* (eds Esposito, L.W., Stofan, E. R. & Cravens, T. E.) 73–100 (American Geophysical Union, 2007).
20. Kasting, J. F., Whitmire, D. P. & Reynolds, R. T. Habitable zones around main sequence stars. *Icarus* **101,** 108–128 (1993).
21. Yung, Y. L. & DeMore, W. B. *Photochemistry of Planetary Atmospheres* (Oxford Univ. Press, 1999).
22. Madhusudhan, N. & Seager, S. A temperature and abundance retrieval method for exoplanet atmospheres. *Astrophys. J.* **707,** 24–39 (2009).
23. Deming, D. *et al*. Discovery and characterization of transiting super earths using an all-sky transit survey and follow-up by the James Webb space telescope. *Publ. Astron. Soc. Pacif.* **121,** 952–967 (2009).
24. Beichman, C. A., Woolf, N. J. & Lindensmith, C. A. *The Terrestrial Planet Finder (TPF): A NASA Origins Program to Search for Habitable Planets* (NASA Jet Propulsion Laboratory, 1999).
25. Von Paris, P., Hedelt, P., Selsis, F., Schreier, F. & Trautmann, T. Characterization of potentially habitable planets: Retrieval of atmospheric and planetary properties from emission spectra. *Astron. Astrophys.* **551,** A120 (2013).
26. Des Marais, D. J. *et al*. Remote sensing of planetary properties and biosignatures on extrasolar terrestrial planets. *Astrobiology* **2,** 153–181 (2002).
27. Han, T. T., Ping, J. S. & Zhang, S. J. Global features and trends of the tropopause derived from GPS/CHAMP RO data. *Sci. China* **54,** 365–374 (2011).
28. Moroz, V. I. & Zasova, L. V. VIRA-2: A review of inputs for updating the Venus International Reference Atmosphere. *Adv. Space Res.* **19,** 1191–1201 (1997).

Acknowledgements

This work was performed as part of the NASA Astrobiology Institute's Virtual Planetary Laboratory, supported by the National Aeronautics and Space Administration through the NASA Astrobiology Institute under solicitation No. NNH05ZDA001C. T.D.R. gratefully acknowledges support from an appointment to the NASA Postdoctoral Program at NASA Ames Research Center, administered by Oak Ridge Associated Universities. D.C.C. was also supported by NASA Exobiology/Astrobiology grant NNX10AQ90G. The authors thank the late C. Leovy for discussions in which he was supportive of pursuing the idea that a 0.1 bar tropopause constitutes an emergent law.

Author contributions

T.D.R. and D.C.C. made equally important contributions to the project and co-wrote the paper. T.D.R. generated the model outputs.

Additional information

Supplementary information is available in the online version of the paper. Reprints and permissions information is available online at www.nature.com/reprints. Correspondence and requests for materials should be addressed to T.D.R.

Competing financial interests

The authors declare no competing financial interests.

nature geoscience

SUPPLEMENTARY INFORMATION

DOI: 10.1038/NGEO2020

Common 0.1 bar tropopause in thick atmospheres set by pressure-dependent infrared transparency

Authors: T. D. Robinson, D. C. Catling

Section S.1. Analytic Tropopause Minimum Optical Depth and Temperature

A radiative region typically extends from the radiative convective boundary through the upper troposphere and through the stratosphere (Fig. 2, main text). Our radiative-convective model is described in Robinson and Catling (2012), and the temperature profile in the radiative portion is given by equation (18) of that paper as:

$$\sigma T^4\left(\tau_{IR}\right)=\frac{F^{\odot}_{strato}}{2}\left[1+\frac{D}{k_{strato}}+\left(\frac{k_{strato}}{D}-\frac{D}{k_{strato}}\right)e^{-k_{strato}\tau_{IR}}\right]+ \frac{F^{\odot}_{tropo}}{2}\left[1+\frac{D}{k_{tropo}}+\left(\frac{k_{tropo}}{D}-\frac{D}{k_{tropo}}\right)e^{-k_{tropo}\tau_{IR}}\right]+\frac{F_i}{2}\left(1+D\tau_{IR}\right) \quad \text{(S1)}$$

Here, σ is the Stefan-Boltzmann constant, T is temperature, τ_{IR} is the grey infrared optical depth, and the other terms were defined in the main text of this paper. Typically, k_{tropo} tends to be small, as this term represents a ratio between the shortwave and infrared optical depths in the troposphere, and the latter tends to be much larger than the former in the troposphere. Thus, we omit tropospheric shortwave attenuation (see Section S.1.1 for a full justification using a sensitivity study), and equation (S1) simplifies to

$$\sigma T^4\left(\tau_{IR}\right)=\frac{F^{\odot}_{strato}}{2}\left[1+\frac{D}{k_{strato}}+\left(\frac{k_{strato}}{D}-\frac{D}{k_{strato}}\right)e^{-k_{strato}\tau_{IR}}\right]+\frac{F^{\odot}_{tropo}+F_i}{2}\left(1+D\tau_{IR}\right). \quad \text{(S2)}$$

Taking the derivative of this expression with respect to τ_{IR}, and setting the resulting expression equal to zero to find a minimum value in the temperature profile, gives

$$\tau_{tp} = \frac{1}{k_{strato}} \ln\left[\frac{F^{\odot}_{strato}}{F^{\odot}_{tropo} + F_i} \left(\frac{k^2_{strato}}{D^2} - 1 \right) \right]. \quad \text{(S3)}$$

The temperature at this value of τ_{IR} is then given by

$$\sigma T^4 \left(\tau_{tp} \right) = \frac{F^{\odot}_{strato}}{2} \left(1 + \frac{D}{k_{strato}} \right) + \frac{F^{\odot}_{tropo} + F_i}{2} \left(1 + \frac{D}{k_{strato}} + \frac{D}{k_{strato}} \ln\left[\frac{F^{\odot}_{strato}}{F^{\odot}_{tropo} + F_i} \left(\frac{k^2_{strato}}{D^2} - 1 \right) \right] \right), \quad \text{(S4)}$$

The tropopause temperature can be used to evaluate the strength of the temperature inversion by comparing this to the stratopause temperature using $\tau_{IR} = 0$ in equation (S2),

$$\sigma T^4 \left(\tau_{IR} = 0 \right) = \frac{F^{\odot}_{strato}}{2} \left(1 + \frac{k_{strato}}{D} \right) + \frac{F^{\odot}_{tropo} + F_i}{2}. \quad \text{(S5)}$$

A measure of the strength of the temperature inversion is then given by:

$$\frac{T(\tau_{IR} = 0) - T(\tau_{tp})}{T(\tau_{tp})} =$$

$$\left[\frac{F^{\odot}_{strato} \left(1 + \frac{k_{strato}}{D} \right) + F^{\odot}_{tropo} + F_i}{F^{\odot}_{strato} \left(1 + \frac{D}{k_{strato}} \right) + \left(F^{\odot}_{tropo} + F_i \right) \left(1 + \frac{D}{k_{strato}} + \frac{D}{k_{strato}} \ln\left[\frac{F^{\odot}_{strato}}{F^{\odot}_{tropo} + F_i} \left(\frac{k^2_{strato}}{D^2} - 1 \right) \right] \right)} \right]^{1/4} - 1 \quad \text{(S6)}$$

Figure S1 shows contours of the strength of the temperature inversion over the same range of parameter space as Fig. 3a (main text). From Fig. 3a, we see that the tropopause optical depth falls off very rapidly for combinations of parameters that approach the threshold limit for tropopause formation (shown as the dashed line). The strength of the temperature inversion for these cases is extremely small (<1%, as shown in Fig. S1), so that the stratospheres for these worlds would be observed as nearly isothermal. Thus, while these

cases do not adhere to our rule of $\tau_{tp} \approx 0.05$, they can be reasonably dismissed because they have virtually no stratospheric inversions or tropopause minima and so do not fall in the class of atmospheres under consideration.

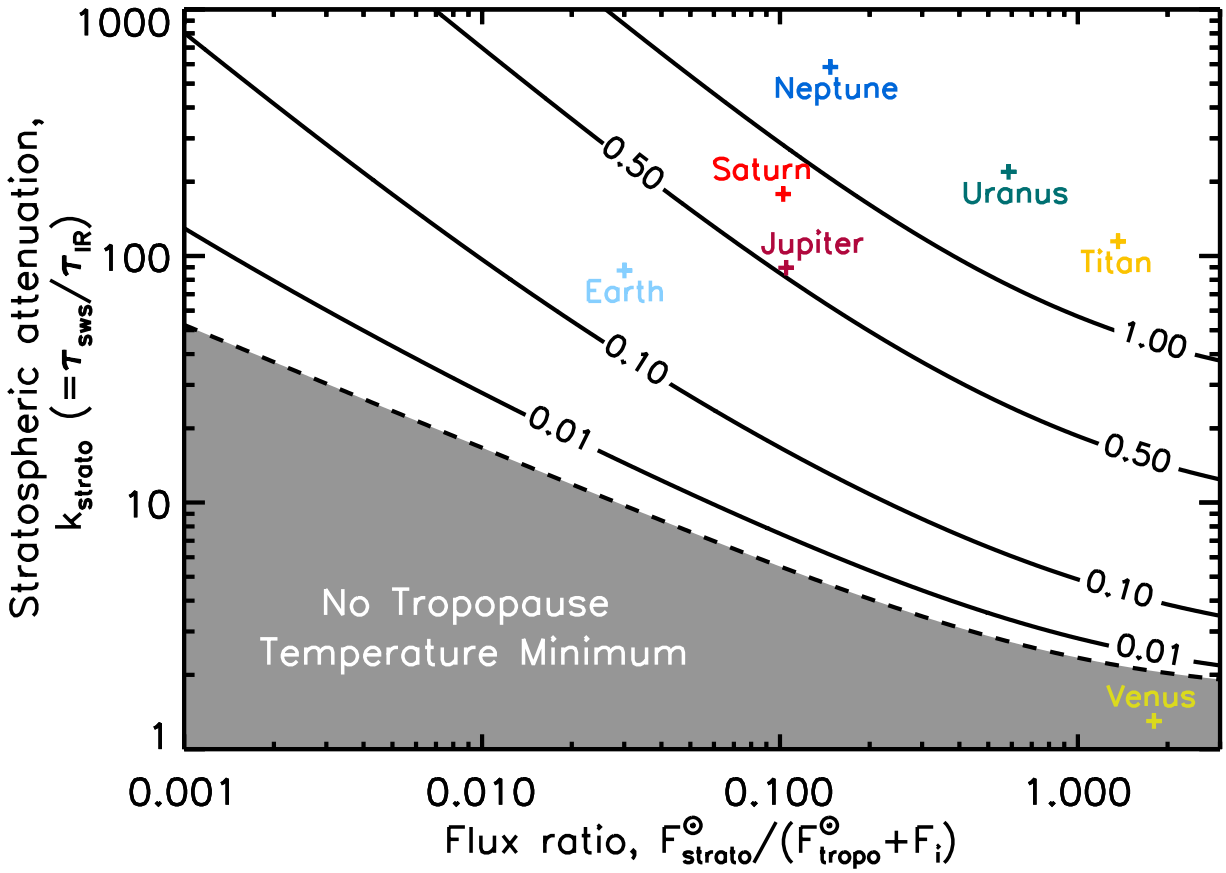

Figure S1 | Contours of the strength of the stratospheric temperature inversion. *The strength of the inversion is the ratio of the difference between the stratopause temperature and the tropopause temperature to the tropopause temperature. This is given by equation (S6), which is a function of the stratospheric attenuation parameter k_{strato} and the ratio of the stellar flux absorbed in the stratosphere ($F^{\odot}_{strato}$) to the sum of the stellar flux absorbed in the troposphere (and surface for planets with surfaces) and the internal heat flux $\left(F^{\odot}_{tropo}+F_i\right)$. The dashed line marks the threshold for tropopause temperature minima, as discussed in the main text.*

Section S.1.1. Sensitivity of the Tropopause Optical Depth to k_{tropo}

Our omission of attenuation of sunlight in our tropospheric channel in deriving the above equations is justified by noting that k_{tropo} is small. This parameter is a ratio of the tropospheric shortwave optical depth to the infrared optical depth, and the latter tends to be much larger than the former in the deep atmosphere. Thus, terms of order k_{tropo} and $k_{tropo}\tau_{IR}$ in equation (S1) are small.

We note that the tropopause optical depth in equation (S3) is most sensitive to the value of k_{tropo} in the limit that both (1) the net tropospheric solar flux absorbed is much larger than the net internal heat flux (i.e., $F^{\odot}_{tropo} \gg F_i$) and (2) $k_{tropo} \lesssim D$. For the former condition, the tropospheric solar channel will dominate the temperature profile and therefore shortwave absorption in the troposphere becomes more important. For the latter, values of k_{tropo} that are nearly equal to D cause the deep atmosphere to go isothermal (for $F^{\odot}_{tropo} \gg F_i$) and add additional absorption of sunlight at high altitudes (low pressures), which can influence where the minimum occurs in the radiative equilibrium temperature profile.

Figure S2 demonstrates how including attenuation in the tropospheric channel affects the infrared optical depth of the tropopause temperature minimum. We choose two values of k_{tropo} / D (0.4 and 0.75) and show contours of $D\tau_{tp}$. Note that these values of k_{tropo} are over three times larger than the most extreme values seen in the Solar System (see Table 1 in the main text, where Titan has $k_{tropo} / D = 0.13$). We also choose the most conservative scenario, wherein $F_i = 0$, so that the shape of the radiative equilibrium temperature profile

in the deep atmosphere is determined solely by the shortwave solar tropospheric channel. Comparing these to the equivalent plot in Fig. 3 (main text) shows that the value of τ_{tp} is relatively insensitive to k_{tropo}.

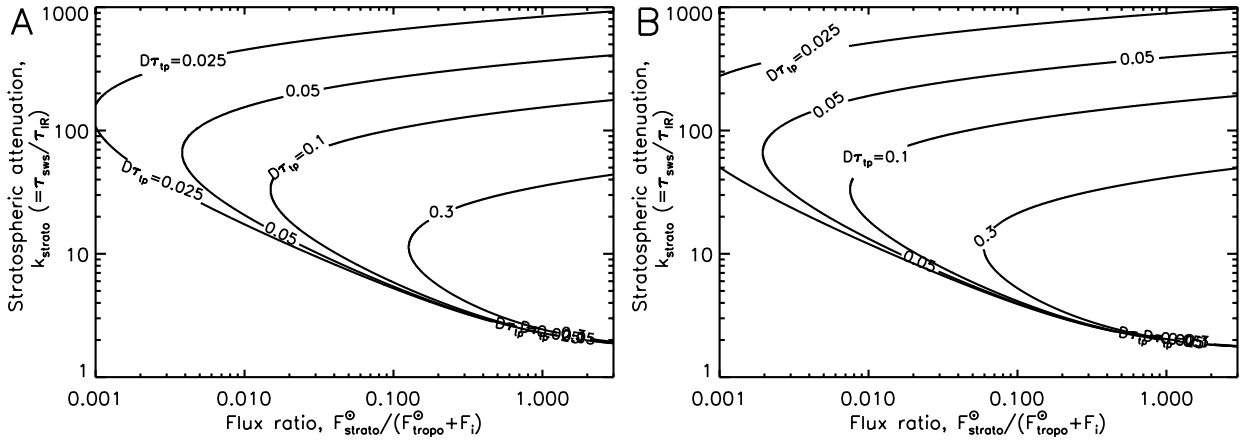

Figure S2 | Influence of k_{tropo} on tropopause optical depth. *Contours are the scaled tropopause infrared optical depth, $D\tau_{tp}$, for two values of k_{tropo}/D (***A***: $k_{tropo}/D = 0.4$;* **B***: $k_{tropo}/D = 0.75$) in the limit that $F_i = 0$. Values of $D\tau_{tp}$ do not change substantially from the case where $k_{tropo} = 0$ (Fig. 3a in the main text), and remain near 0.1 over a very wide range of parameter space.*

Section S.1.2. How the Stratospheric Attenuation Coefficient k_{strato} Affects Heating

In our model, k_{strato} controls the shape of the net shortwave flux profile for the stratospheric channel. Since the atmospheric heating rate is proportional to the rate of change of the net flux, k_{strato} also affects our model heating rate profiles. Typically, the well-known Chapman function describes the atmospheric heating from radiation absorbed by a uniformly distributed absorber (Seinfeld & Pandis 1998, p. 149), and has the heating rate (in temperature change per unit time) as an exponentially decreasing function of pressure. As the following derivation shows, our model has the same relationship between pressure

and heating rate when we use parameters that are appropriate for upper atmospheres. In essence, attenuation is negligible at high altitudes because although there is high light intensity in the shortwave, there is a tiny number density of absorber. The exponential increase of the absorber density with increasing pressure dominates the overall shortwave absorption in the upper atmosphere and causes the exponential increase in absorption with declining altitude, which we have parameterized. (Also see Sindhu (2006) for a discussion of the physics of radiation absorption by gases.)

Our model thus assumes that shortwave radiation is exponentially attenuated in the stratosphere, and we write the net flux in the stratospheric channel as $F^{\odot}_{strato}\exp\left(-\tau_{sws}\right)$, where τ_{sws} is the shortwave optical depth. We then assume that τ_{sws} is proportional to τ_{IR}, so that

$$F^{\odot}_{strato}e^{-\tau_{sws}} = F^{\odot}_{strato}e^{-k_{strato}\tau_{IR}} \qquad \text{(S7)}$$

Thus k_{strato}, the constant of proportionality, controls the attenuation strength and vertical distribution of the shortwave flux absorbed in the stratospheric channel.

The heating rate for the stratospheric channel, Q_{strato}, is proportional to the rate of change of the net flux with respect to height, and is given by

$$Q_{strato}\left(\tau_{IR}\right) = \frac{1}{c_p\rho}\frac{d}{dz}F^{\odot}_{strato}\,\mathrm{e}^{-k_{strato}\tau_{IR}} = \frac{-k_{strato}}{c_p\rho}F^{\odot}_{strato}\,\mathrm{e}^{-k_{strato}\tau_{IR}}\frac{d\tau_{IR}}{dz}, \qquad \text{(S8)}$$

where c_p is the specific heat, ρ is the atmospheric density and $d\tau_{IR}/dz$ is negative, so that the heating rate is a positive quantity. Using the hydrostatic equation, we can further expand this relationship as

$$Q_{strato}\left(\tau_{IR}\right)=\frac{-k_{strato}}{c_p\rho}F^{\odot}_{strato}\,\mathrm{e}^{-k_{strato}\tau_{IR}}\frac{d\tau_{IR}}{dp}\frac{dp}{dz}=\frac{gk_{strato}}{c_p}F^{\odot}_{strato}\,\mathrm{e}^{-k_{strato}\tau_{IR}}\frac{d\tau_{IR}}{dp}, \qquad \text{(S9)}$$

where g is the gravitational acceleration and p is atmospheric pressure. Finally, using our power law relationship between τ_{IR} and pressure, $\tau_{IR}=\tau_0\left(p/p_0\right)^n$ (see Section S.2), we can express the heating rate profile in terms of τ_{IR} as

$$Q_{strato}\left(\tau_{IR}\right)=\frac{gk_{strato}}{c_p}\frac{n\tau_0^{1/n}}{p_0}\tau_{IR}^{(n-1)/n}F^{\odot}_{strato}\,\mathrm{e}^{-k_{strato}\tau_{IR}}, \qquad \text{(S10)}$$

or in terms of pressure as

$$Q_{strato}\left(p\right)=\frac{gk_{strato}}{c_p}\frac{n\tau_0}{p_0^n}p^{n-1}F^{\odot}_{strato}\,\mathrm{e}^{-k_{strato}\tau_0\left(p/p_0\right)^n}. \qquad \text{(S11)}$$

For the case of $n=1$, which is appropriate for the middle and upper stratosphere, the heating rate is simply an exponential in pressure, which is the same as the aforementioned Chapman function. From these expressions we can clearly see how k_{strato} controls the heating rate profile—low values of k_{strato} distribute the heating over a large portion of the column, while large values of k_{strato} concentrate the heating at very low pressures (i.e., high in the atmosphere).

More realistic models of the Solar System worlds investigated in the main text, which assumed $n=2$ throughout the profile, would transition to $n=1$ in the middle stratosphere. While such a transition alters the thermal structure of the upper atmosphere, it does not significantly affect the inferred tropopause pressure. This is because the tropopause

occurs in the regime where pressure broadening and/or collision-induced absorption dominate the opacity, and, thus, $n = 2$ applies.

For some Solar System worlds (e.g., Titan, Earth), the shortwave absorbers that are responsible for causing a stratospheric inversion are not uniformly distributed. In these cases, the associated heating rate is not an exponentially decreasing function of pressure. Nevertheless, our formalism can still reproduce the thermal structure of such atmospheres by using a value for k_{strato} that effectively captures the average atmospheric heating rate. Thus, our exploration of a very wide range of parameter space for k_{strato} in the main text serves to investigate a large distribution of potential atmospheric heating scenarios.

Section S.2. Relating Infrared Optical Depth τ_{IR} and Pressure

While the vertical coordinate of the equations governing the transfer of thermal radiation is optical depth, the natural physical vertical coordinate of planetary atmospheres is pressure. Thus, in order to relate the tropopause optical depth to the tropopause pressure, we must relate the grey infrared optical depth (τ_{IR}) to atmospheric pressure.

The grey infrared differential optical depth, $d\tau_{IR}$, across an atmospheric layer of thickness dz with N distinct sources of opacity (e.g., various absorbing gases) is defined by

$$d\tau_{IR} = -\sum_{i=1}^{N} \kappa_i \rho_i dz \qquad \text{(S12)}$$

where κ_i is the grey opacity (expressed as a mass extinction coefficient) from the i^{th} source, which generally depends on pressure and temperature, and ρ_i is the mass density

of the i^{th} opacity source, which also depends on pressure. If we denote the mass mixing ratio of species i as w_i, then the mass density of the species can be written as

$$\rho_i = w_i \rho \tag{S13}$$

so that equation (S12) can be written as

$$d\tau_{IR} = -\sum_{i=1}^{N} \kappa_i w_i \rho dz \,. \tag{S14}$$

In hydrostatic equilibrium, we have

$$\frac{dp}{dz} = -g\rho \tag{S15}$$

where p is atmospheric pressure and g is the gravitational acceleration. Solving for ρdz and inserting this into equation (S14) yields

$$d\tau_{IR} = \sum_{i=1}^{N} \kappa_i w_i \frac{dp}{g} \,. \tag{S16}$$

If we represent the mass mixing ratio profile and opacity of an absorber as

$$w_i(p) = w_i(p_0)\left(\frac{p}{p_0}\right)^{a_i} \tag{S17}$$

$$\kappa_i(p) = \kappa_i(p_0)\left(\frac{p}{p_0}\right)^{b_i} \tag{S18}$$

where p_0 is the pressure at some reference level in the atmosphere, then equation (S16) reads

$$d\tau_{IR} = \sum_{i=1}^{N} \kappa_i(p_0) w_i(p_0)\left(\frac{p}{p_0}\right)^{a_i+b_i} \frac{dp}{g} \tag{S19}$$

which can be simplified further if either (1) the opacity is dominated by a single source (e.g., water vapor in Earth's lower troposphere), (2) the atmosphere has multiple

absorbers that have similar pressure dependences in their opacities and vertical distributions (e.g., N_2 and CH_4 in Titan's atmosphere), or (3) the mixing ratios and opacities have been combined into a weighted-mean opacity (replacing the sum over $\kappa_i w_i$ with a single value of κ) then we can write a proportionality from equation (S19) as

$$d\tau_{IR} \propto \left(\frac{p}{p_0} \right)^{a+b} dp \qquad \text{(S20)}$$

or

$$\tau_{IR} = \tau_0 \left(\frac{p}{p_0} \right)^{n} \qquad \text{(S21)}$$

where τ_0 is the grey infrared optical depth integrated down from the top of the atmosphere to the reference pressure, and

$$n = a + b + 1 . \qquad \text{(S22)}$$

In the simplest case, when an absorbing gas is well mixed ($a = 0$) and the opacity does not depend strongly on pressure ($b = 0$), then we will have $n = 1$, which physically corresponds to Doppler broadening in the upper stratosphere or higher. For tropospheres and lower stratospheres, a very common scenario is to have a well mixed gas ($a = 0$) providing collision-induced opacity (e.g., H_2 in gas giant atmospheres in the Solar System), which gives $b = 1$, so that $n = 2$. Typically, n takes a value between 1 and 2, as has been parameterized into some models (Heng et al. 2012). Figure S3 demonstrates the effects of changing *n* in our thermal structure models for Titan and Jupiter (results for Saturn, Uranus, and Neptune are similar to Jupiter, and so are omitted). In all cases, the model with

$n = 2$ produces the most realistic troposphere, tropopause, and lower stratosphere, which are the regions emphasized in this study.

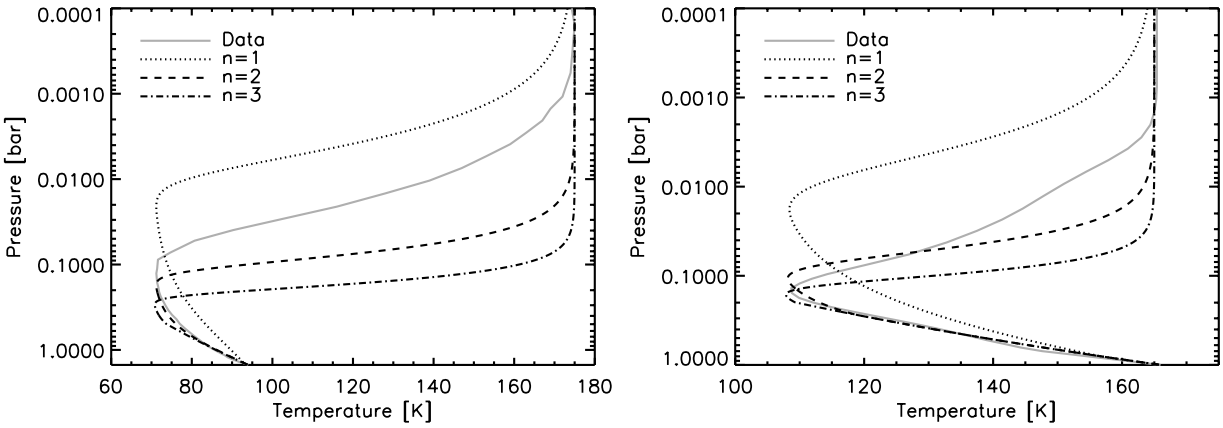

Figure S3 | Influence of *n* on models of atmospheric thermal structure for Titan (left) and Jupiter (right). *Models with n*=1, 2, *and* 3 *are explored, and compared to data (grey). In general, cases with n*=2 *produce the most realistic troposphere, tropopause, and lower stratosphere, as theory predicts. Theory also predicts that an upward transition to n=1 would provide a better match for the upper stratosphere where Doppler broadening dominates, as has been shown previously (Robinson & Catling 2012).*

For Earth, water vapor is the primary opacity source in the lower troposphere, and its vertical profile depends strongly on pressure due to condensation at the colder temperatures of the middle and upper troposphere. To capture this strong dependence on pressure, some authors have proposed that n=4–5 in equation (S21) in Earth's troposphere (Goody 1954, p. 170; Weaver & Ramanathan 1995; Satoh 2004, p. 373; Frierson et al. 2006). However, we use n=2 because our calculations show that it better captures the infrared fluxes of the troposphere as a whole, as follows. It also has a common physical basis in pressure-broadening and collision-induced absorption (main text) that is more

general for planetary tropospheres than a consideration of purely Earth-like atmospheric compositions.

To determine the accuracy of our Earth models and of models with steeper τ-p scalings, we ran an accurate, line-by-line (LBL) simulation of the upwelling and downwelling thermal infrared fluxes in a cloud-free Earth atmosphere (Meadows & Crisp 1996). We assumed standard mean atmospheric compositions and temperatures (McClatchey et al. 1972) in the LBL model. For the comparison, we used three different grey and windowed-grey parameterizations of the infrared radiative transport, and all of these used the same temperature profile as the LBL model. For the grey calculations, the free parameters are the τ-p scaling and the total grey infrared optical depth of the atmosphere, τ_0. One of the grey calculations corresponds to this work, with n=2 throughout the entire troposphere and with τ_0=1.9 (see main text Table 1). The second grey calculation is from Frierson, et al. (2006), who take n=4 in the deep troposphere, transitioning to n=1 at about 0.5 bar, and who use an average τ_0 of 2.9. The windowed-grey model is from Weaver and Ramanathan (1995), and adds an additional parameter, which is the fraction of the total infrared spectrum that is transparent to thermal radiation, β. For this model, we assume the same τ-p scaling and τ_0 as Frierson, et al. (2006), and take β=0.25, which is the fraction of flux from a 288 K blackbody that escapes between 8–12 μm.

Figure S4 shows the comparison between these four models. The n=2 model reproduces the fluxes from the LBL calculation at least as well as, and often better, than other models. The pure grey model with n=4 in the deep troposphere does not accurately reproduce the

LBL fluxes, and, most notably, yields downwelling infrared fluxes at the surface that are about 20% (60 W/m^2) too large. Adding a window to the latter model improves the fit but not substantially compared to the simpler n=2 model. In reality, thermal radiative transport in Earth's atmosphere is complex, with a steep (n=4–5) τ-p scaling for the 6.3 μm water band and the water rotational bands beyond about 20 μm, a window between 8–12 μm, and a n=2 scaling for the 15 μm CO_2 band. Our model, with n=2 throughout the troposphere turns out to be a reasonable approximation despite this complexity.

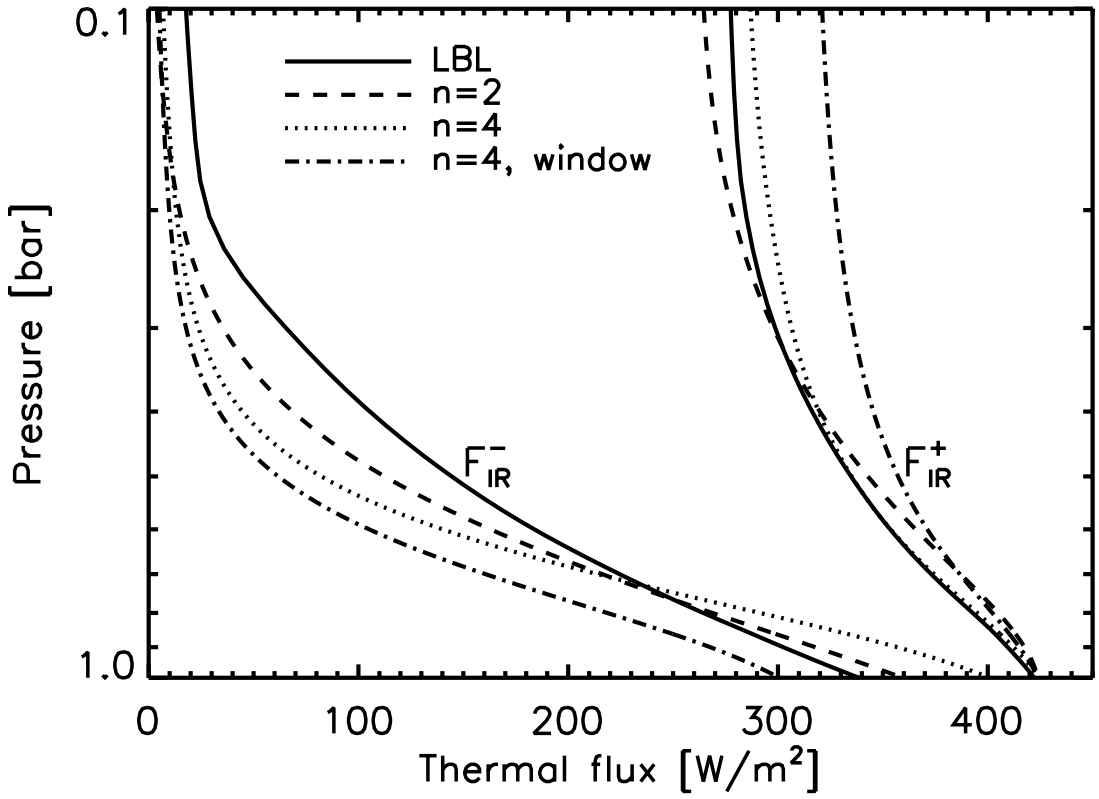

Figure S4 | Accuracy of different radiative transport parameterizations. *Upwelling and downwelling infrared fluxes are shown for a standard mean Earth atmosphere for: (1) a line-by-line (LBL) radiative transport model (solid), (2) the model used in this work, which is grey and assumes n=2 for the $\tau \propto p^n$ scaling (dashed), (3) a grey model that assumes n=4 in the deep atmosphere (dotted), and (4) a windowed-grey model that also assumes n=4 in the deep atmosphere (dash-dotted).*

Finally, we note that if Earth warmed substantially, and the 8–12 μm window region closed because of opacity from water vapor continuum absorption, models show that the atmospheric structure becomes governed by the water saturation vapor pressure curve and the planet enters a "runaway greenhouse" state (Abe & Matsui 1988; Kasting 1988; Nakajima et al. 1992; Goldblatt & Watson 2012). In such an unstable state, the radiative-convective boundary moves to high altitudes at pressures << 0.1 bar for surface temperatures above ~350 K. We do not consider hypothetical atmospheres such as these that are climatically unstable in time. Instead, our discussion of the tropopause level applies to stable, long-lived atmospheres with stratospheric inversions, i.e., those we observe.

Section S.3. Infrared Optical Depths at 1 bar in Hypothetical but Plausible Planetary Atmospheres

Our power law relationship between grey infrared optical depth and pressure yields a 0.1 bar tropopause if the infrared optical depth τ_0 is of order a few at a reference pressure p_0 of 1 bar. The value of the tropopause pressure scales weakly with τ_0 ($p_{tp} \propto \tau_0^{-1/2}$), and our modeling results for the Solar System yield $2 \leq \tau_0 \leq 10$. Here, we extend our calculations of the infrared optical depth at 1 bar to three broad categories: Titan-like worlds, gas giants, and terrestrial worlds. Results are shown in Fig. S5, and are discussed below.

Our Titan-like worlds possess N_2-dominated atmospheres with 5-10% CH_4 and trace amounts of H_2. We assume an isothermal temperature structure, which is sufficient to

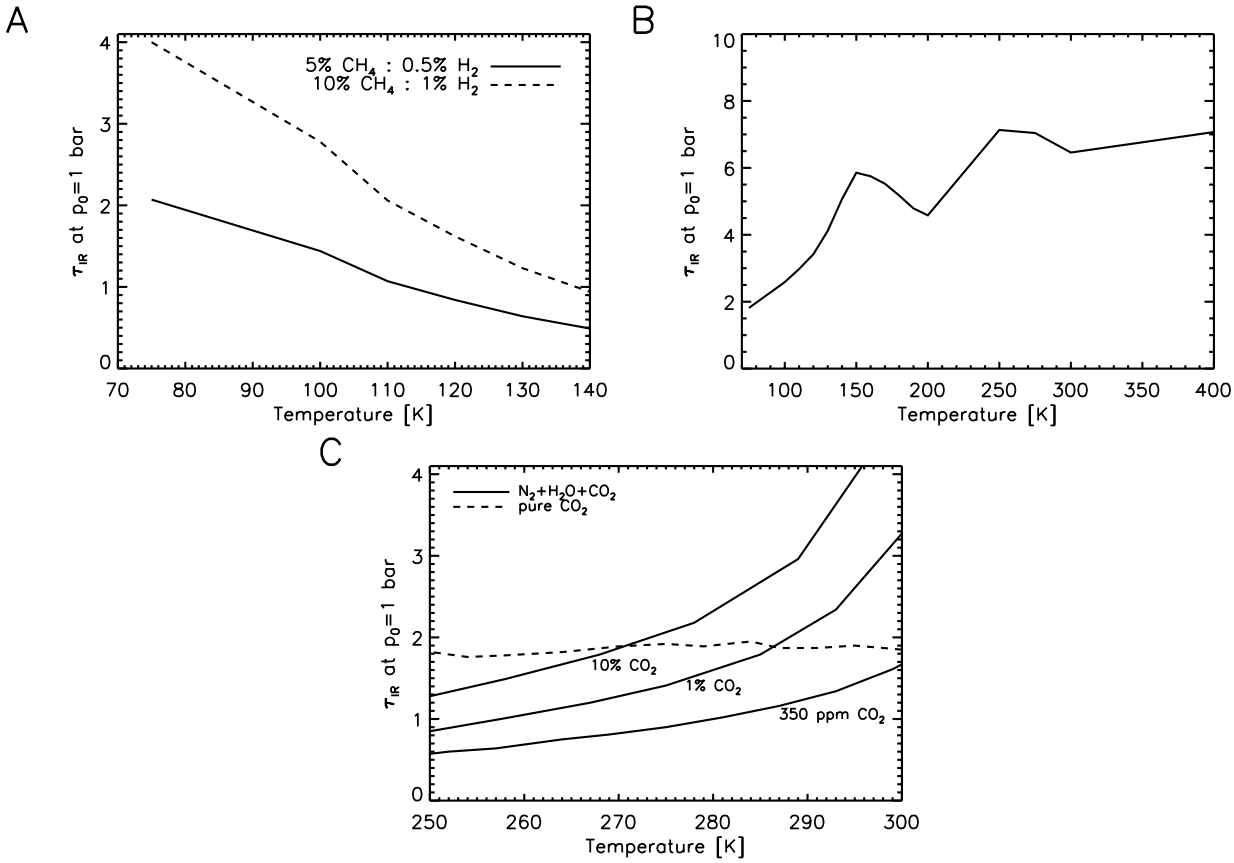

Figure S5 | Grey infrared optical depth at 1 bar in several categories of planetary atmospheres. (**A**) *A Titan-like case, where the atmosphere is predominantly N_2, and has either 5% CH_4 and 0.5% H_2 (solid) or 10% CH_4 and 1% H_2 (dashed).* (**B**) *A Jupiter-like case, where temperature dependent opacities are taken from Freedman et al. (2008).* (**C**) *Terrestrial cases, with atmospheres of N_2, H_2O, and various CO_2 amounts (solid lines), and for a pure CO_2 atmosphere (dashed).*

understand the infrared optical depths for these worlds. Opacity is provided by collision-induced absorption from the following pairs: N_2-N_2, N_2-CH_4, CH_4-CH_4, and N_2-H_2 (Borysow & Frommhold 1986b, 1986a, 1987; Borysow & Tang 1993). We compute Rosseland mean optical depths using a line-by-line radiative transfer model, and our values agree with

those of McKay et al. (1997) for Titan's tropospheric temperatures of ~90. For a wide range of temperatures, our Titan-like worlds are optically thick in the infrared with $1 \leq \tau_0 \leq 4$. The case with 5% CH_4 and 0.5% H_2 has optical depths below unity at temperatures above 115 K. However, assuming 5% CH_4 in a 1 bar atmosphere at these temperatures is likely too conservative because the saturation vapor pressure of methane at 115 K is 1.3 bar. We did not compute values above 140 K as carbon dioxide can begin to volatilize at these temperatures.

The gas giant cases in Fig. S5 use temperature-dependent Rosseland mean opacities from Freedman, et al. (2008), assume isothermal atmospheres and a Jupiter-like gravity of 25 m/s^2. These models have $2 \leq \tau_0 \leq 7$ for temperatures between 75–400 K. For Saturn- or Neptune-like worlds, with smaller gravities and enhanced metallicities, we would expect that the optical depths increase. Unfortunately, the Freedman et al. results do not extend to the metallicities appropriate for such investigations.

The terrestrial cases in Fig. S5 assume atmospheres of either pure CO_2 or a mixture of N_2, H_2O, and CO_2. Temperature structures for the various cases were computed using a 1-D, cloud-free radiative-convective model designed for application to terrestrial planets (Kasting & Ackerman 1986; Haqq-Misra et al. 2008). The cases with 10% and 1% CO_2 assume that the troposphere is saturated with respect to water vapor, and that the stratosphere has a constant mixing ratio of water that is set by a tropopause cold trap temperature. The case with 350 ppm CO_2 (appropriate for modern Earth) is more Earth-like, and assumes a relative humidity distribution from Manabe and Wetherald (1967).

Grey thermal optical depths were determined by fitting the numerical models with the analytic radiative-convective model used in the Solar System cases in the main text (Robinson & Catling 2012). The temperature indicated along the horizontal axis is the surface temperature from the numerical model.

A pure CO_2 atmosphere has $\tau_0 \sim 2$ at 1 bar for temperatures between 250–300 K. At temperatures lower than about 250 K, CO_2 begins to condense in the atmosphere, which will significantly affect atmospheric structure and the greenhouse effect (Kasting et al. 1993; Forget & Pierrehumbert 1997). Thus, investigating τ_0 values in colder pure CO2 atmospheres would require more complex models that include cloud microphysics, which is beyond the scope of this work.

Optical depths at l bar for the N_2-H_2O-CO_2 cases depend strongly on temperature and, to a lesser extent, the assumed CO_2 concentration. For the 10% CO_2 case, we have $1 \leq \tau_0 \leq 4$ for temperatures between 250–300 K. At high temperatures, atmospheric water vapor concentrations are large, which drives up the optical depth values. At colder temperatures, water vapor is a very trace gas, and larger CO_2 concentrations are required to keep the optical depth above unity. An active carbonate-silicate cycle should prevent a terrestrial planet from having low CO_2 concentrations at cold temperatures (Walker et al. 1981), so that the pure CO_2 value of $\tau_0 \sim 2$ is more realistic for cold worlds with thick atmospheres.

The Earth-like case in Fig. S5, with 350 ppm CO_2 case and a surface temperature of 288 K, has τ_0=1.1. This can be compared to the result we get when applying our model to Earth in

the main text, which gives τ_0=1.9. This difference is due to the absence of cloud greenhouse effects in the Kasting et al. climate model, which, as a result, must absorb more solar flux to maintain a 288 K surface temperature. We deduce this by noting that, in the Kasting et al model, the Bond albedo for a planet at 1 AU from a Sun-like star and with an Earth-like atmospheric composition is 0.23, while Earth's known Bond albedo is 0.30. Thus, the Earth-like case in the Kasting et al. model absorbs an additional 24 W/m^2 of solar flux than the actual Earth's 240 W/m^2 and so needs less greenhouse effect than our model to generate the same surface temperature. This added solar flux in the Kasting et al. model compensates, in part, for Earth's longwave cloud forcing, which is about 30 W/m^2 (Ramanathan et al. 1989). This means that the τ_0 values in Fig. S5(c) are systematically somewhat lower than they should be.

Section S.4. The Role of Hazes in Determining Stratospheric Infrared Optical Depths

Stratospheric and mesospheric hazes in all planetary atmospheres of the Solar System are essentially transparent to thermal infrared radiation, which is an important condition for inversions and tropopause minima in our proposed rule. Here we demonstrate why this is likely a generality. In short, haze particles need to be ~1 μm size (or larger) to interact with thermal radiation. Gravitational settling and coagulation of such large particles generally limit the thermal infrared optical depth of very high altitude hazes to << 1.

To show this limitation, we developed a simple model of haze microphysics. The model assumes a bi-modal distribution of aerosols—small particles that are generated high in the stratosphere, and large particles that form from the small particles and which, due to their

larger size, can provide infrared opacity. Both modes evolve due to gravitational settling and coagulation. Let $n_h(z)$ be the number density profile (in particles per unit volume) of either mode of haze particles in our model. Then, the time rate of change of the number density is given by

$$\frac{dn_h}{dt} = -\frac{d\phi}{dz} + q \qquad \text{(S23)}$$

where $\phi = \phi(z)$ is the particle flux (in particles per unit area per unit time), z is altitude, and $q = q(z)$ is the particle production rate profile (in particles per unit volume per unit time, and where a negative production rate represents destruction). Thus, in steady state, we have

$$\frac{d\phi}{dz} = q \ , \qquad \text{(S24)}$$

which simply states that the flux gradient is balanced by particle creation or loss.

Settling controls the particle flux in our model, and is given by

$$\phi = -vn_h \, , \qquad \text{(S25)}$$

where v is the settling speed. In the low-pressure conditions found in stratospheres, particles experience Epstein drag, and their terminal velocity is given by (Epstein 1924)

$$v = \left(\frac{\pi}{8mk_BT} \right)^{1/2} \frac{\rho_h g r_h}{n} \, , \qquad \text{(S26)}$$

where m is the mean atmospheric molecular mass, k_B is Boltzmann's constant, T is temperature, ρ_h is the density of the haze substance, g is the acceleration due to gravity, r_h is the radius of a haze particle, and n is the atmospheric gas number density (in molecules per unit volume). With the simplifying approximation that temperature and gravity are

independent of height, all of the terms in equation (S26) except for *n* can be combined into one altitude-independent parameter (with units of flux), given by

$$\eta = \left(\frac{\pi}{8 m k_B T} \right)^{1/2} \rho_h g r_h \qquad \text{(S27)}$$

or, after inserting typical values,

$$\eta = 5.6 \times 10^{20} \, \mathrm{m^{-2} s^{-1}} \left(\frac{m}{4.6 \times 10^{-26} \, \mathrm{kg}} \right)^{-1/2} \left(\frac{T}{200 \ \mathrm{K}} \right)^{-1/2} \left(\frac{\rho_h}{1 \ \mathrm{g/cm^3}} \right) \left(\frac{g}{10 \ \mathrm{m/s^2}} \right) \left(\frac{r_h}{1 \ \mu\mathrm{m}} \right). \qquad \text{(S28)}$$

Thus, we write the settling speed for particles as

$$v = \frac{\eta}{n}, \qquad \text{(S29)}$$

which gives a settling speed of 1.5×10^{-2} m/s at 0.01 bar for particles of radius 10 μm, such that particles of this size are expected to rain out quickly, falling 10 km in a matter of days.

In an isothermal atmosphere the number density *n* varies as $dn/dz = -n/H$, where *H* is the scale height ($H = k_B T / mg$). Inserting this, as well as our expressions for settling, and using the ideal gas law and the hydrostatic equation, into equation (S24) gives

$$\frac{df_h}{dp} = \frac{H}{\eta} \frac{q}{p}, \qquad \text{(S30)}$$

where we have defined the haze particle number density mixing ratio, $f_h = n_h / n$, and we have shifted to using atmospheric pressure, *p*, as the vertical coordinate. This differential equation is straightforward to solve for our two different particle modes, which will each have a different functional form for *q*, the production rate profile.

Once the particle number density profiles have been determined, the infrared optical depth can be computed given definition of optical depth for particles

$$d\tau_{IR} = -Q_{ext}\pi r_h^2 n_h dz \ , \qquad \text{(S31)}$$

where Q_{ext} is a grey particle extinction efficiency. Using the equation for hydrostatic equilibrium, equation (S31) can be written

$$d\tau_{IR} = \frac{Q_{ext}\pi r_h^2}{g}\frac{n_h}{\rho}dp = \frac{Q_{ext}\pi r_h^2}{mg} f_h dp \ . \qquad \text{(S32)}$$

We now discuss solving equations (S30) and (S32) for our two particle modes.

Section S.4.1. Number Densities and Optical Depths for Particle Modes

Smaller particles in our model are generated aloft, and are destroyed by coagulating to form particles in the larger mode. The destruction of these particles is given by

$$q_1 = -K_{c1} n_{h1}^2 \qquad \text{(S33)}$$

where a sub-script "1" now refers to the small mode, and K_{c1} is the particle coagulation coefficient (typically of order 10^{-9} cm^3/s/particle for a 0.1 μm sized particle). Inserting this into equation (S30), and using the definition of the particle mixing ratio and the ideal gas law, we have

$$\frac{df_{h1}}{dp} = -\frac{H}{\eta_1}\frac{K_{c1} n_{h1}^2}{p} = -\frac{H}{\eta_1}\frac{K_{c1} f_{h1}^2 n^2}{p} = -\frac{K_{c1}}{\eta_1 g m k_B T} p f_{h1}^2 \ . \qquad \text{(S34)}$$

To solve equation (S34), we need a boundary condition, so we simply set the haze number density for the small mode to a constant, n_{ht}, at some pressure p_t (the sub-script '*t*' is for the *top* of the haze column). We take n_{h1} to be zero above p_t, and we will investigate a wide

range of values for these boundary conditions in Sec. S.4.2. In terms of mixing ratio, the number density boundary condition is given by

$$f_{ht} = f_h(p_t) = \frac{n_{ht}}{n(p_t)} = \frac{k_B T n_{ht}}{p_t}. \quad \text{(S35)}$$

Integrating equation (S34) using this boundary condition, we obtain

$$f_{h1}(p) = \frac{f_{ht}}{1 + \frac{K_{c1} f_{ht}}{2\eta_1 g m k_B T}\left(p^2 - p_t^2\right)}. \quad \text{(S36)}$$

Converting from mixing ratios to number densities, we have an analytic expression for the number density profile of the small mode:

$$n_{h1}(p) = \frac{p}{\frac{p_t}{n_{ht}} + \frac{K_{c1}}{2\eta_1 g m}\left(p^2 - p_t^2\right)}. \quad \text{(S37)}$$

Note that $n_{h1} = 0$ for $p < p_t$. An analytic solution for the infrared optical depth profile for the small mode can be determined by inserting f_{h1} from equation (S36) into equation (S32) and integrating to find

$$\tau_{IR1}(p) = \frac{2}{\pi}\tau_\infty \left[\tan^{-1}\left(\frac{p}{\sqrt{p_t\left(p_* - p_t\right)}} \right) - \tan^{-1}\left(\frac{p_t}{\sqrt{p_t\left(p_* - p_t\right)}} \right) \right], \quad \text{(S38)}$$

where we have defined a constant with units of pressure

$$p_* = \frac{2\eta_1 g m}{K_{c1} n_{ht}}, \quad \text{(S39)}$$

and a limiting optical depth

$$\tau_\infty = \frac{Q_{ext}\pi^2 r_{h1}^2 k_B T n_{ht}}{2mg} \sqrt{\frac{p_*^2}{p_t\left(p_* - p_t\right)}}, \quad \text{(S40)}$$

which is the value of equation (S38) in the limit that p_t is small and when $p \to \infty$.

Large-mode particles in our model are created from the coagulation of small-mode particles, and are destroyed via coagulation. The production profile is then given by

$$q_2 = -K_{c2} n_{h2}^2 + \left(\frac{r_{h1}}{r_{h2}} \right)^3 K_{c1} n_{h1}^2 \ , \qquad \text{(S41)}$$

where K_{c2} is the coagulation coefficient for the large size mode. Note that the latter term is the production from the coagulation of smaller particles, for which it takes $\left(r_{h1} / r_{h2} \right)^{-3}$ small particles to create one large particle, assuming identical density and a spherical shape. We determine the number densities of the large mode numerically. This is done by inserting equation (S41) into equation (S30), and using the analytic form of $n_{h1}(p)$ from equation (S37). The boundary condition is that $n_{h2}(p) = 0$ at the top of the atmosphere. Finally, infrared optical depths for this mode are numerically evaluated from equation (S32).

Section S.4.2. Infrared Optical Depths for a Wide Range of Potential Haze Conditions

To determine the range of potential infrared optical depths due to stratospheric hazes, we ran our simple model over a wide range of parameter space for the variables p_t and n_{ht}. The other parameters in our investigation are gravity (g), atmospheric mean molecular mass (m), atmospheric temperature (T), haze density (ρ_h), grey particle extinction efficiency (Q_{ext}), and the size (r_h) and coagulation coefficient (K_c) for the small and large size modes.

In the following studies, we use $\rho_h = 1$ g/cm^3, and we make the conservative assumption of $Q_{ext} = 2$. For the large-mode particles, we take $r_{h2} = 1$ μm and $K_{c2} = 3 \times 10^{-10}$ cm^3/s

(Kulkarni et al. 2011, p. 37). Particles of this size are large enough to provide substantial infrared opacity (which goes as $n_h r_h^2$), while small enough to avoid large settling speeds.

First, we consider a scenario where the small-mode particles are relatively small ($r_{h1} = 0.01$ μm) and are created at low pressures (high altitudes), as is typically the case for organic hazes in the Solar System (Rages et al. 1991; Toon et al. 1992; Lavvas et al. 2008). For these aerosols, we take $K_{c1} = 1 \times 10^{-9}$ cm^3/s. Figure S6(a) shows contours of the stratospheric infrared optical depth for a Titan-like case, with $g = 1.4$ m/s^2, $m = 4.6 \times 10^{-26}$ kg/molecule (appropriate for pure N_2), and $T = 170$ K. A Jupiter-like case with $g = 25$ m/s^2 and $m = 3.3 \times 10^{-27}$ kg/molecule (appropriate for pure H_2) is not significantly different since the decrease in the molecular weight counters the effects from the increase in gravity. In both cases the optical depths are dominated by the small-mode particles, since it is difficult to form many large-mode particles from the smaller particles.

Second, we consider a case where the small-mode particles are larger ($r_{h1} = 0.1$ μm) and are created at higher pressures (lower altitudes), which is more analogous to Venus (Wilquet et al. 2009). Figure S6(b) shows contours of the stratospheric infrared optical depth for this scenario, with $K_{c1} = 7 \times 10^{-10}$ cm^3/s (Kulkarni, et al. 2011, p. 37), $g = 10$ m/s^2, $m = 7.2 \times 10^{-26}$ kg/molecule, and $T = 200$ K. Note that these parameters are appropriate for an Earth-sized terrestrial planet with a CO_2-dominated atmosphere.

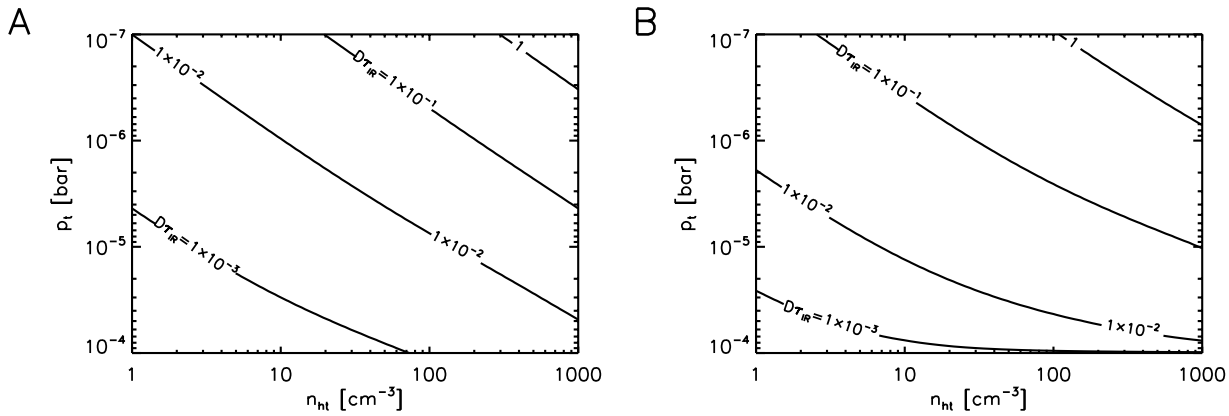

Figure S6 | Grey infrared optical depths at 0.1 bar in hazy stratospheres. *Results are from our simple bi-modal model. For both cases, we take* $\rho_h = 1$ *g/cm³, and we make the conservative assumption of* $Q_{ext} = 2$ *. For the large-mode particles, we take* $r_{h2} = 1$ *μm and* $K_{c2} = 3\times10^{-10}$ *cm³/s.* (**A**) *A Titan-like case, with* $g = 1.4$ *m/s²,* $m = 4.6\times10^{-26}$ *kg/molecule (appropriate for pure* N_2*), and* $T = 170$ *K. The optical depths are typically very small, and are primarily due to the small-mode particles, which have* $r_{h1} = 0.01$ *μm and* $K_{c1} = 1\times10^{-9}$ *cm³/s.* (**B**) *A case more similar to Venus, with* $g = 10$ *m/s²,* $m = 7.2\times10^{-26}$ *kg/molecule (appropriate for pure* CO_2*), and* $T = 200$ *K. The small-mode particles are larger than in (a), and have* $r_{h1} = 0.1$ *μm and* $K_{c1} = 7\times10^{-10}$ *cm³/s.*

In general, our models show that it is very difficult for stratospheric hazes to achieve infrared optical thickness, with $\tau_{IR} \ll 1$ over most of parameter space. The large-mode particles, which provide most of the infrared opacity, are limited to relatively small number densities by coagulation and rain-out, thus preventing them from achieving substantial optical depths. Only in the scenarios where a very large number of small-mode particles are created at very low pressures can relatively large infrared optical depths be achieved.

However, these cases are unphysical as placing large amounts of haze material at such low pressures yields mass mixing ratios that are over an order of magnitude larger than those seen in the haziest of stratospheres. For example, Titan has stratospheric haze mass mixing ratios of order 1 ppm (Toon, et al. 1992), while the top-right of Figures S6(a) and S6(b) have ~20 ppm.

We note that certain combinations of n_{ht} and p_t in our model can lead to stratospheric hazes that are opaque in the infrared when temperatures are very high ($T \gtrsim 1000$ K) and the mean atmospheric molecular weights are low. However, worlds that meet these temperature and composition criteria are rare (Howard et al. 2010), and studies of HD 189733b, a Hot Jupiter that may possess a stratospheric haze, indicate that the condensate particles are both small and in low number densities, making them poor infrared opacity sources (Lecavelier des Etangs et al. 2008). Future work that is beyond the scope of our simple model could investigate the importance of diffusion, which will more strongly affect smaller particles due to their lower settling speeds.

Section S.5. Venus: A Test Case of k_{strato} Determining whether a Tropopause Occurs

The global average temperature profile for Venus possesses an extremely weak or non-existent tropopause temperature minimum. However, latitudinally-resolved retrievals of the thermal structure of the Venusian atmosphere show a distinct tropopause temperature minimum near 0.1 bar at high latitudes, between 55° and 85° (Tellmann et al. 2009). The location of this temperature minimum is thus consistent with our 0.1 bar tropopause rule.

Explanations for this Venusian "cold collar inversion" have invoked enhancements in shortwave absorbers relative to the global mean (Taylor et al. 1983), but interpretation is complicated because of the presence of unknown absorbers at 0.2–0.5 μm (Mills et al. 2007). Some authors have also argued that the inversion is due to thermal radiative processes (Schubert et al. 1980). Ultimately, the reason for the latitudinal variations in tropopause sharpness is not fully understood, but is commonly believed to be a modulation of the radiative-convective mean state by a Hadley-like meridional circulation above the cloud tops (Newman et al. 1984; Baker & Leovy 1987). This circulation could generate an inversion through adiabatic heating in the descending portion of the circulation (Crisp 1983). All of these mechanisms can be incorporated into our simple model; variations in shortwave absorption or longwave thermal processes can be represented in our k_{strato} parameter, while adiabatic heating in the upper atmosphere is represented, in effect, by an increase in the ratio $F^{\odot}_{strato} / \left(F^{\odot}_{tropo} + F_i \right)$.

To investigate the Venusian tropopause, we first derived a profile of the grey infrared optical depth using the global-average aerosol properties and distributions from Crisp (1989), which is shown in Fig. S7(a). From this figure we see that the Venusian radiative-convective boundary, which occurs on average near 0.2–0.3 bar (Tellmann, et al. 2009), is located at an optical depth of τ_{IR}~2–3. This is consistent with the generalized thermal structure presented in the primary manuscript where τ_{IR} is always unity or greater at the radiative-convective boundary (Fig. 2). We also see that the Venusian high-latitude 0.1 bar tropopause occurs at a relatively large infrared optical depth of τ_{tp}~0.4, compared to the other thick atmospheres of the Solar System (Table 1, main text).

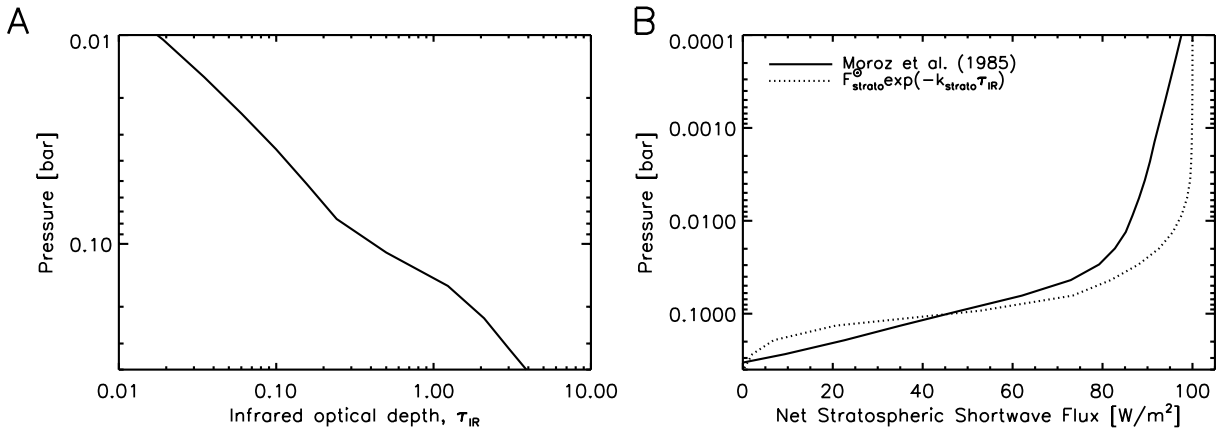

Figure S7 | Global average profiles of infrared optical depth (A) and net shortwave stratospheric flux (B) for Venus. *The pressure range in* (**A**) *highlights the region near the tropopause (~0.1 bar) and radiative-convective boundary (~0.2 bar). The solid line in* (**B**) *is taken from the models of Moroz et al. (1985), while the dotted line is a fit of the form* $F^{\odot}_{strato}\exp\left(-k_{strato}\tau_{IR}\right)$*, with* k_{strato}*=1.3.*

Models of the global-average net shortwave flux for Venus show that roughly 100 W/m^2 is absorbed in the upper atmosphere (Moroz, et al. 1985; Titov et al. 2007), primarily by aerosols. Thus, $F^{\odot}_{strato}/\left(F^{\odot}_{tropo}+F_i\right)\sim 1.8$, assuming that F_i is negligible and a Bond albedo of 0.76 (Moroz, et al. 1985). Using the inequality from the main text for the development of a tropopause temperature minimum $\left(k^2_{strato} > D^2\left[1+\left(F^{\odot}_{tropo}+F_i\right)/F^{\odot}_{strato}\right]\right)$, this flux ratio indicates that a value of $k_{strato} \gtrsim 2$ is required for the development of a tropopause temperature minimum on Venus.

Combining the profile of net shortwave flux absorbed in the Venusian stratosphere with the infrared optical depth profile in Fig. S7(a) gives a best-fit, global average value of k_{strato}~1.3, and the associated flux profile for this value of k_{strato} is shown in Fig. S7(b). This

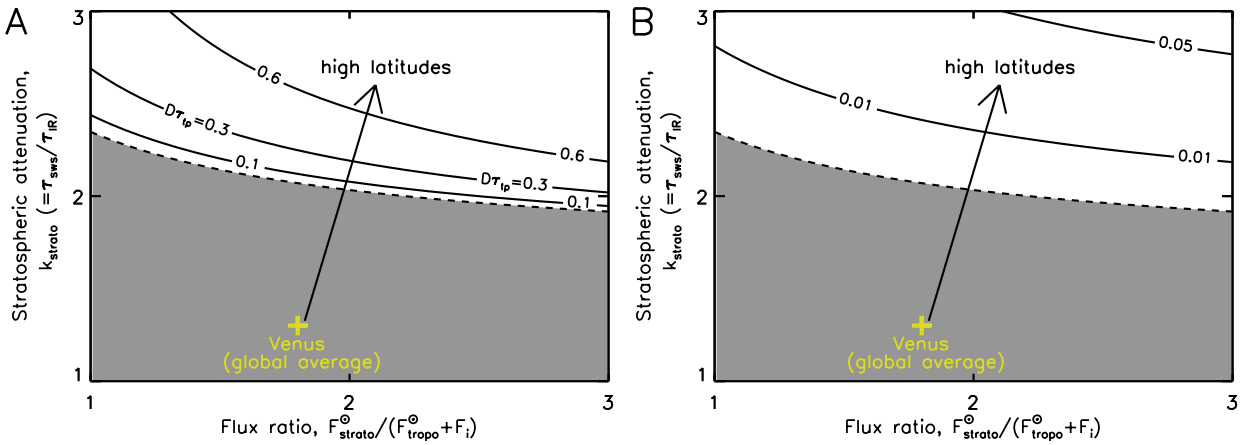

Figure S8 | Depiction of how the Venusian high latitudes develop a tropopause temperature minimum. *Changes at high latitudes to the stratospheric shortwave or infrared opacities could increase k_{strato}, while adiabatic heating from downwelling air could increase the flux ratio, $F^{\odot}_{strato}/\left(F^{\odot}_{tropo}+F_i\right)$. In these scenarios, the Venusian high-latitudes could develop a tropopause temperature minimum at a relatively large infrared optical depth (***A***; contours tropopause optical depths, highlighting a region of main text Fig. 3a) with a weak inversion (***B***; contours inversion strengths highlighting a region of Fig. S1).*

value of k_{strato} places Venus at the lower-right of main-text Fig. 3(a), indicating that Venus, in the global average, is on the cusp of having a tropopause temperature minimum. However, in the high-latitudes of Venus, an increase in k_{strato} (representing an increase in stratospheric shortwave absorption or decrease in infrared opacity) or an increase in $F^{\odot}_{strato}$ (representing an increase in heating due to dynamical processes) would lead to a more strongly developed tropopause temperature minimum. Modest increases in these parameters would yield a tropopause temperature minimum at a relatively large infrared optical depth with a weak inversion strength (<10%), which are demonstrated schematically in Fig. S8. These values are consistent with the high-latitude tropopause

infrared optical depths of ~0.4 and observed inversion strengths, defined in equation (S6), of ~1–6% (Tellmann, et al. 2009).

Section S.6. Sources for Temperature Profile and Model Parameter Data

Pressure-temperature profiles in Fig. 1 (main text) are from: Moroz and Zasova (1997) (Venus), McClatchey, et al. (1972) (Earth), Moses et al. (2005) (Jupiter), Lindal et al. (1983) (Titan) and Lindal (1992) (Saturn, Uranus and Neptune).

Reference pressures and temperatures (p_0 and T_0, respectively) in Table 1 (main text) are from the aforementioned data for atmospheric thermal structure. Observed mean tropopause pressures are from: Sausen and Santer (2003) (Earth), McKay, et al. (1997) (Titan), Lindal (1992)(Jupiter and Uranus), Del Genio et al. (2009) (Saturn) and Bishop et al. (1995) (Neptune). Our dry-adiabat adjustment parameters, α, which accounts for condensation of volatiles, were deduced from: Peixoto and Oort (1992) (Earth), Strobel et al. (2009) (Titan) and Irwin (2009) (Jupiter, Saturn, Uranus and Neptune).

The solar flux absorbed in the stratosphere and troposphere ($F^{\odot}_{strato}$ and $F^{\odot}_{tropo}$, respectively) for Earth and Titan were taken from Hartmann (1994) and McKay et al. (1991), respectively. As these parameters are not well-measured for the gas and ice giants, we took the appropriate values from the atmospheric thermal structure models of Fortney et al. (2011). While these models do not include clouds and hazes, they still accurately reproduce the observed thermal structure of the giants, as neglecting dark hazes and bright clouds tend to offset one another. Internal heat fluxes (F_i) are from: Hanel et al. (1981)

(Jupiter), Hanel et al. (1983) (Saturn), Pearl et al. (1990) (Uranus) and Pearl and Conrath (1991) (Neptune).

The stratospheric and tropospheric solar attenuation parameters (k_{strato} and k_{tropo}) indicate the ratio between the shortwave and infrared optical depths in these two regions of the atmosphere. The value of k_{strato} was chosen so that the model radiative equilibrium temperature at the top of the atmosphere matched the observed stratospheric temperature maximum from each of the respective sets of thermal structure data. Note that this temperature is determined by setting τ_{IR} to zero in equation (S1). We take the tropospheric solar attenuation parameter to be given by

$$k_{tropo} = \frac{\ln\left(F^{\odot}_{tropo} / \left(F^{\odot}_{tropo} - F^{\odot}_{tropo,p_0}\right)\right)}{\tau_0} \qquad \text{(S42)}$$

where $F^{\odot}_{tropo,p_0}$ is the solar flux absorbed in the troposphere above the reference pressure p_0, so that the natural log term is the shortwave optical depth in the troposphere.

As an example, for Earth, where p_0 = 1 bar is the surface, $F^{\odot}_{strato} = 7$ W/m^2 corresponds to the shortwave flux absorbed by ozone in the stratosphere, and $F^{\odot}_{tropo} = 233$ W/m^2 corresponds to the flux absorbed in the troposphere and at the surface. The sum of these two fluxes is 240 W/m^2, which is equal to the net solar flux absorbed by Earth accounting for a Bond albedo of 0.30. Water vapor absorbs a significant amount of solar flux in Earth's troposphere so that $F^{\odot}_{tropo,p_0} = 60$ W/m^2, which is included in the 233 W/m^2 total. Thus, the

tropospheric shortwave optical depth is $\ln\left(F^{\odot}_{tropo} / \left(F^{\odot}_{tropo} - F^{\odot}_{tropo,p_0}\right)\right)$ = ln(233/(233-60)) and equation (S42) gives a value of $k_{tropo} = 0.16$ for $\tau_0 = 1.9$.

Finally, the grey infrared optical depths of the radiative-convective boundary (τ_{rc}) and the reference level (τ_0) are determined by the model by requiring that the temperature and upwelling thermal flux are both continuous at the radiative-convective boundary (Robinson & Catling 2012). The grey infrared optical depth of the tropopause temperature minimum (τ_{tp}) can then be deduced from the model temperature profile, and is related to the tropopause pressure through $p_{tp} / p_0 \approx (\tau_{tp} / \tau_0)^{0.5}$ (main text equation 3), as discussed in Section S.2.

Section S.7. Stratospheric Absorbers and Coolers

The chemistry of oxidizing or reducing stratospheres gives rise to common shortwave absorbers and coolers, which are shown in Table S1. Because the infrared optical depth is small in stratospheres, the shortwave absorbers dominate the heating and cause temperature inversions. On Venus, the chemistry of the shortwave absorber and whether it has a role in stratospheric inversions is presently unknown (see Sec. S.5). However, mid to high latitude profiles on Venus that have tropopause minima (unlike the global mean) satisfy the ~0.1 bar tropopause rule despite this lack of knowledge, which is a reassuring test of the generality of our proposed rule.

Table S1 | Molecules responsible for stratospheric shortwave heating and infrared cooling in thick atmospheres of the Solar System.

World	Stratospheric heating	Stratospheric cooling
Oxidizing stratospheres:		
Venus	unknown absorber (UV), CO_2, sulfur-bearing aerosols	CO_2, sulfur-bearing aerosols
Earth	ozone	CO_2
Reducing stratospheres		
Jupiter	aerosols (UV/vis), CH_4 (NIR)	acetylene (C_2H_2), ethane (C_2H_6)
Saturn	aerosols (UV/vis), CH_4 (NIR)	acetylene (C_2H_2), ethane (C_2H_6)
Titan	haze, CH_4 (NIR)	acetylene (C_2H_2), ethane (C_2H_6), haze
Uranus	aerosols (UV/vis), CH_4 (NIR)	acetylene (C_2H_2), ethane (C_2H_6)
Neptune	aerosols (UV/vis), CH_4 (NIR)	acetylene (C_2H_2), ethane (C_2H_6)

References:

Abe, Y., & Matsui, T. 1988, J Atmos Sci, 45, 3081

Baker, N. L., & Leovy, C. B. 1987, Icarus, 69, 202

Bishop, J., Atreya, S. K., Romani, P. N., Orton, G. S., Sandel, B. R., & Yelle, R. V. 1995. in Neptune and Triton, The middle and upper atmosphere of Neptune (University of Arizona Press), 427

Borysow, A., & Frommhold, L. 1986a, The Astrophysical Journal, 311, 1043

---. 1986b, The Astrophysical Journal, 303, 495

---. 1987, The Astrophysical Journal, 318, 940

Borysow, A., & Tang, C. 1993, Icarus, 105, 175

Crisp, D. 1983, Ph.D. thesis, Princeton

---. 1989, Icarus, 77, 391

Del Genio, A. D., Achterberg, R. K., Baines, K. H., Flasar, F. M., Read, P. L., Sánchez-Lavega, A., & Showman, A. P. 2009, Saturn from Cassini-Huygens, 1, 113

Epstein, P. S. 1924, Phys Rev, 23, 710

Forget, F., & Pierrehumbert, R. T. 1997, Science, 278, 1273

Fortney, J. J., Ikoma, M., Nettelmann, N., Guillot, T., & Marley, M. S. 2011, The Astrophysical Journal, 729, 32

Freedman, R. S., Marley, M. S., & Lodders, K. 2008, The Astrophysical Journal Supplement Series, 174, 504

Frierson, D. M. W., Held, I. M., & Zurita-Gotor, P. 2006, J Atmos Sci, 63, 2548

Goldblatt, C., & Watson, A. J. 2012, Philosophical Transactions of the Royal Society A: Mathematical, Physical and Engineering Sciences, 370, 4197

Goody, R. M. 1954, The physics of the stratosphere (CUP Archive)

Hanel, R., Conrath, B., Kunde, V., Pearl, J., & Pirraglia, J. 1983, Icarus, 53, 262

Hanel, R. A., Conrath, B. J., Herath, L. W., Kunde, V. G., & Pirraglia, J. A. 1981, J Geophys Res, 86, 8705

Haqq-Misra, J. D., Domagal-Goldman, S. D., Kasting, P. J., & Kasting, J. F. 2008, Astrobiology, 8, 1127

Hartmann, D. L. 1994, Global physical climatology (San Diego: Academic Press)
Heng, K., Hayek, W., Pont, F., & Sing, D. K. 2012, Mon Not R Astron Soc, 420, 20
Howard, A. W., et al. 2010, Science, 330, 653
Irwin, P. 2009, Giant planets of our solar system: Atmospheres, composition, and structure (2nd ed.; Chichester, UK: Springer)
Kasting, J. F. 1988, Icarus, 74, 472
Kasting, J. F., & Ackerman, T. P. 1986, Science, 234, 1383
Kasting, J. F., Whitmire, D. P., & Reynolds, R. T. 1993, Icarus, 101, 108
Kulkarni, P., Baron, P. A., & Willeke, K. 2011, Aerosol Measurement: Principles, Techniques, and Applications (Wiley)
Lavvas, P., Coustenis, A., & Vardavas, I. 2008, Planetary and Space Science, 56, 67
Lecavelier des Etangs, A., Pont, F., Vidal-Madjar, A., & Sing, D. 2008, Astronomy and Astrophysics, 481, 83
Lindal, G. F. 1992, Astron J, 103, 967
Lindal, G. F., Wood, G. E., Hotz, H. B., Sweetnam, D. N., Eshleman, V. R., & Tyler, G. L. 1983, Icarus, 53, 348
Manabe, S., & Wetherald, R. T. 1967, Journal of Atmospheric Sciences, 24, 241
McClatchey, R. A., Fenn, R. W., Selby, J. E. A., Volz, F. E., & Garing, J. S. 1972, in (Air Force Cambridge Research Labs)
McKay, C. P., Martin, S. C., Griffith, C. A., & Keller, R. M. 1997, Icarus, 129, 498
McKay, C. P., Pollack, J. B., & Courtin, R. 1991, Science, 253, 1118
Meadows, V. S., & Crisp, D. 1996, J Geophys Res, 101, 4595
Mills, F. P., Esposito, L. W., & Yung, Y. L. 2007, in Exploring Venus as a Terrestrial Planet, eds. L. W. Esposito, E. R. Stofan, & T. E. Cravens (Washington, D. C.: American Geophysical Union), 73
Moroz, V. I., et al. 1985, Advances in Space Research, 5, 197
Moroz, V. I., & Zasova, L. V. 1997, Advances in Space Research, 19, 1191
Moses, J. I., Fouchet, T., Bézard, B., Gladstone, G. R., Lellouch, E., & Feuchtgruber, H. 2005, Journal of Geophysical Research (Planets), 110, 8001
Nakajima, S., Hayashi, Y. Y., & Abe, Y. 1992, J Atmos Sci, 49, 2256
Newman, M., Schubert, G., Kliore, A. J., & Patel, I. R. 1984, Journal of Atmospheric Sciences, 41, 1901
Pearl, J. C., & Conrath, B. J. 1991, J Geophys Res, 961, 18921
Pearl, J. C., Conrath, B. J., Hanel, R. A., Pirraglia, J. A., & Coustenis, A. 1990, Icarus, 84, 12
Peixoto, J. P., & Oort, A. H. 1992, Physics of Climate (New York: American Institute of Physics)
Rages, K., Pollack, J. B., Tomasko, M. G., & Doose, L. R. 1991, Icarus, 89, 359
Ramanathan, V., Cess, R., Harrison, E., Minnis, P., Barkstrom, B., Ahmad, E., & Hartmann, D. 1989, Science (New York, NY), 243, 57
Robinson, T. D., & Catling, D. C. 2012, The Astrophysical Journal, 757, 104
Satoh, M. 2004, Atmospheric circulation dynamics and general circulation models (Chichester, UK: Praxis Pub.)
Sausen, R., & Santer, B. D. 2003, Meteorol Z, 12, 131
Schubert, G., et al. 1980, J Geophys Res, 85, 8007
Seinfeld, J. H., & Pandis, S. N. 1998, Atmospheric Chemistry and Physics (New York: J. Wiley and Sons)

Sindhu, P. S. 2006, Fundamentals of Molecular Spectroscopy (New Age International (P) Limited)
Strobel, D. F., et al. 2009, in Titan from Cassini-Huygens, eds. R. H. Brown, J.-P. Lebreton, & J. H. Waite (New York: Springer), 235
Taylor, F., Hunten, D., & Ksanfomaliti, L. 1983, Venus, 1, 650
Tellmann, S., Patzold, M., Hausler, B., Bird, M. K., & Tyler, G. L. 2009, J Geophys Res, 114
Titov, D. V., Bullock, M. A., Crisp, D., Renno, N. O., Taylor, F. W., & Zasova, L. V. 2007, Geophysical Monograph-American Geophysical Union, 176, 121
Toon, O., McKay, C., Griffith, C., & Turco, R. 1992, Icarus, 95, 24
Walker, J. C. G., Hays, P. B., & Kasting, J. F. 1981, J Geophys Res, 86, 9776
Weaver, C. P., & Ramanathan, V. 1995, J Geophys Res, 100, 11585
Wilquet, V., et al. 2009, J Geophys Res, 114, E00B42